Dynamics of river plumes in coastal ocean

Peter Zavialov*, Victor Zhurbas and Alexander Osadchiev

P.P.Shirshov Institute of Oceanology,
Russian Academy of Sciences
*E-mail: peter@ocean.ru

Abstract

The paper is focused on specific aspects of the dynamics of river plumes in the coastal oceans, namely, their response to the wind forcing and interaction with the baroclinic circulations associated with the upwellings and downwellings.

A numerical simulation is used to investigate the process of the transport of the river runoff by alongshore baroclinic sea currents. This part of the study is based on the implementation of the Princeton Ocean Model (POM) under the conditions of an idealized circular stratified basin whose surface is exposed to a transient tangential wind stress event to induce an alongshore baroclinic current. A baroclinic current of the downwelling type (i.e., directed to the left to a sea viewing observer in the Northern Hemisphere) was shown to provide the flushing of the river discharge from estuary's vicinity more effectively than that of the upwelling type. This finding of the model experiments is also confirmed by the in situ measurements data.

Furthermore, a Lagrangian model of a surface-advected river plume in the barotropic ocean is developed. The model combines the deterministic approach following from the momentum budget with a random-walk scheme. The model reproduced satisfactorily the general features of the plume dynamics known from previous studies, as well as the *in situ* measurements and satellite imagery. Using the model, we obtained the dependences between the spatial extent of the plume and the wind stress $\boldsymbol{\tau}$. The character of these dependences proved to depend critically on the wind direction with respect to the geometry of the coast and the river mouth. For the offshore and "downwelling-favoring" alongshore winds, the plume area initially grows with the increase of τ, and then starts to decrease when τ exceeds certain critical value. For the onshore wind, the area decreases steadily (though not linearly) as $\boldsymbol{\tau}$ increases. The most complex behavior is observed for the "upwelling-favoring" alongshore wind: the plume area initially decreases until the wind stress exceeds a certain critical value, then starts to increase with $\boldsymbol{\tau}$ and attains a maximum, and then eventually drops to zero as $\boldsymbol{\tau}$ continues to increase.

These results may have practical implications for the transport of pollutants and nutrients in the coastal regions of freshwater influence.

1. Introduction

The continental river discharges supply the ocean with the fresh water; suspended and dissolved terrigenous substances; nutrients; and, not infrequently, anthropogenic pollutants. In total, the average long-term volume of the river runoff into the ocean is believed to be as high as 39000 km^3 per year (Lvovich, 1986), which is close to 12 Sv and makes up about a quarter of the incoming water budget of the ocean (the atmospheric precipitation on the ocean's mirror supplies the remaining three quarters). However, the relative contribution of the continental runoff can be an order of magnitude higher in certain ocean shelf areas and in inland and marginal seas in reference to the ocean as a whole (e.g., Simonov and Altman, 1991). For instance, the annual river runoff into the Black Sea (338 km^3 per year) substantially exceeds the atmospheric precipitation (238 km^3 per year), being close to the magnitude of the evaporation (396 km^3 per year).

Once the river water inflows into the sea, it forms distinct mesoscale structures on the ocean surface adjacent to the river mouth, commonly called "plumes". Salinity within such a structure is, generally, lower than that of the surrounding ocean waters, and many other properties also differ. The horizontal scale of a plume can be of tens and even hundreds of kilometers, and yet the interface between the plume and the sea water often remains as sharp as a few centimeters. River plumes can significantly modify the physical structure of the shelf waters. In the sea areas adjacent to river estuaries, the buoyancy flux from the fluvial discharges can be comparable or even exceed the buoyancy input associated with seasonal heating (Simpson, 1996). The mixing/stirring dynamics in the regions of freshwater influence varies broadly from seasonal stratification pattern (Simpson and Bowers, 1984) to rather complex short-scale (0.5-15 days) variability governed by local winds, ambient sea currents, tides and river inflow dynamics (Simpson, 1996). This is especially true for the plumes of small and medium size rivers because of the small-scale physical processes taking place in the areas influenced by these plumes (e.g., Chao, 1988; Garvine, 1995). Small and medium size rivers are often characterized by rapid flooding events (Nash, 1994), in contrast to large rivers whose variability is normally dominated by seasonal cycling (e.g., Lentz and Limeburner, 1995; Geyer et al., 1996; Simpson, 1996).

The response of plumes to diverse types of wind forcing and the interaction of the former with the background alongshore currents belong to the least studied aspects of the river plumes dynamics in the coastal ocean waters. Only a few works on these aspects were published, and their results sometimes contradict each other. For instance, field observations of the Eel River plume in northern California (USA) during the flood flow in the winters of 1996–1997 and 1997–1998 are reported in (Geyer et al., 2000). These authors established that the downwelling-favorable winds under the flood flow conditions led to a plume appearing as an alongshore strip up to 10 km wide to the right of the river's mouth, while the upwelling-favorable ones forced the plume to move mainly across the shelf and to the left of the mouth. The conclusion concerning the narrowing of the plume under the conditions of the upwelling-favorable winds was also corroborated in (Pullen and Allen, 2000), where numerical simulation was applied to study the behaviour of the same plume of the Eel River during the same time period. Use has been made of the Princeton Ocean Model (Blumberg and Mellor, 1987).

On the other hand, it is interesting to note that Munchow and Garvine (1993), based on the field observations in the mouth of the Delaver River, came earlier to an opposite conclusion: in their view, the plume's effective area increases under upwelling-inducing winds, while the downwelling-inducing winds press the plume to the shore. The same view was repeated in two of the recent papers, namely, in (Choi and Wilkin, 2007), where the plume of the Hudson River (USA) was simulated with the ROMS three-dimensional hydrodynamical model and in (Xia et al., 2007), where the Cape Fear River plume (North Carolina, USA) was examined under different wind conditions based on the EFDC three-dimensional hydrodynamical model (Hamrick, 1992). As stated in the last work, even a weak wind forcing is able to change the direction of motion of a plume, but, at strong winds, the plume rapidly shrinks or vanishes due to mixing.

The present paper is focused on specific aspects of the dynamics of river plumes in the coastal oceans, namely, their response to the wind forcing and interaction with the baroclinic circulations associated with the upwellings and downwellings. In the first part of the study, we investigate how the upwelling or downwelling conditions influence the spatial dispersal and dynamics of a river plume. As mentioned above, the previously published results on this matter are somewhat contradictory. Possibly, this is due to the fact that the previous works considered the "integral" effect without attempting to separate the two substantially different physical mechanisms occurring under the conditions of the upwelling or downwelling events: first, the mechanical wind effects upon the plume and, second, the transfer of the plume by the baroclinic background currents arising from the upwelling (downwelling). Meanwhile, both mechanisms are substantial, and the final result can depend on their superposition. In the first part of this study, we try to eliminate the purely wind effects and to focus our attention on the interaction of a plume and the baroclinic currents. We present the results of numerical experiments with POM in an idealized stratified basin and, next, use the data of the field observations of the plume of the Vulan River in the Black Sea to illustrate the inferences.

In the second part of this paper, we investigate the dynamics of the plume moving solely under the wind forcing. The behavior of plumes under external forcing such as the wind stress or the interaction with an ambient coastal circulation is not fully understood. To this end, we develop a Lagrangian numerical model of a surface-advected river plume. We apply the model and tune it for the plume of Mzymta River in the Black Sea . We use our recent *in situ* measurements to validate the model. Further, using the model, we investigated the dependencies between the spatial extent of the plume and the wind stress $\boldsymbol{\tau}$. The character of these dependencies proved to depend critically on the wind direction with respect to the geometry of the coast and the river mouth.

2. Transport of river runoff by alongshore baroclinic sea current

2.1 Setup of numerical experiments

The Princeton Ocean Model was used for the simulation of the processes of the river runoff transport by the marine currents. The numerical experiments are performed in an idealized round stratified basin with a diameter of $\boldsymbol{D}$ = 60 km. The basin's depth is $\boldsymbol{H}$ = 20 m.The initial salinity field is set to be homogeneous ($\boldsymbol{S(x, y, z)} = \boldsymbol{S_0}$ = 18‰ at $\boldsymbol{t}$ = 0), while the density stratification is governed by the temperature: the initial temperature in the upper and lower 10 m thick layers equals 21°C and 15°C, respectively. To imitate the river runoff, a certain amount of fresh water is added to the upper σ-layer of a grid cell (200 by 200 m) adjacent to the shore line. The alongshore baroclinic current in the round basin was generated in the following way. A tangential wind stress directed along the shore line of the round basin is applied to the water surface. The wind stress is applied for one day only and then is switched off. Next, the calculation of the current field is carried out for the one day period of calm conditions, when the drift component of the current substantially decelerates, and the baroclinic current, being related to the deformation of the density field, becomes dominant. Subsequent to this, the river runoff switches on and the process of its transport by the alongshore baroclinic current begins.

2.2 Upwelling and downwelling conditions

We show below that the river runoff transport by the alongshore baroclinic current strongly depends upon the current direction. In this connection, we distinguish two types of alongshore baroclinic currents, namely, the upwelling and downwelling ones. The currents of the upwelling (downwelling) type are characterized by the shorewards surfacing (descent) of the isopycnals and are directed to the left (right) in reference to an observer viewing the sea in the Northern Hemisphere.

Fig. 1 illustrates the evolution of the surface salinity field in the basin in the presence of the alongshore baroclinic current of the upwelling and downwelling types.

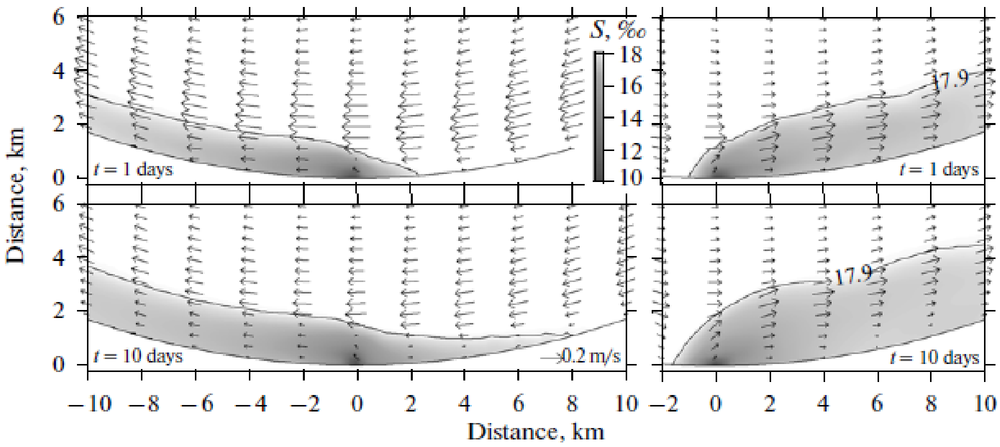

Figure 1: Dispersal of fresh water in a salty basin (with salinity of 18‰) with constant depth (H = 20 m) outflowing from a local source characterized by a discharge rate of Q = 10 m^3/s and located at the shoreline. The figure displays the model maps of the salinity (black-and-white scale) and the current's velocity (arrows) in the presence of the alongshore baroclinic currents of the upwelling (left panels) and downwelling (right panels) types.

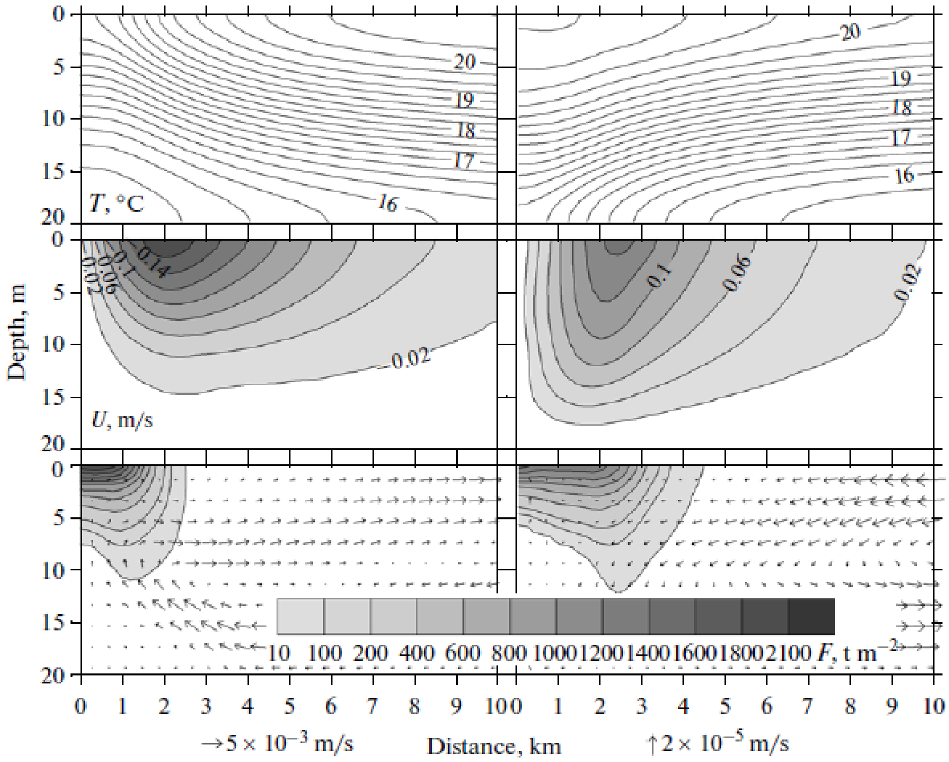

Figure 2: The temperature ***T***, the alongshore component of the current velocity ***U***, and the mass of fresh water per unit of area of the transversal cross section of the basin ***F*** as functions of the depth and the offshore distance at the point in time ***t*** = 10 days in the case of a flat bottom basin. The left hand panels depict the case of a baroclinic current of the upwelling type, while the right hand ones show the same current but of the downwelling type. The arrows show the transversal circulation in the background of the ***F*** cross sections.

The vertical structure of the alongshore baroclinic currents and the respective temperature fronts, as well as the distribution of the river runoff depending on the distance from the shore and on the vertical coordinate, are shown in Fig. 2. This figure displays the spatial structure of the temperature values *T* and the alongshore component of the current velocity *U*, as well as the mass of the fresh water arriving from the river's mouth per unit of area of the basin's cross section *F* at the instant *t* = 10 days.

In order to evaluate the efficiency of the removal of the incoming river water from the near-mouth domain by the alongshore baroclinic current, we used the three-dimensional salinity field to calculate the total volume of river water ***Vol*** contained within the 10 km vicinity of the mouth and plotted its dependence on the ltime *t* after the source is activated. Fig. 3 represents the dependences ***Vol*(*t*)** for the cases of the baroclinic upwelling- and downwelling-type conditions. At $t \leq 0.75$ days, ***Vol*(*t*)** behave in a similar way for all cases : it linearly grows. The further behavior of the dependence ***Vol*(*t*)** radically depends upon the type of the baroclinic current. In the case of the downwelling_type current, at ***t*** > 1 day, ***Vol*** stops growing and a quasi-stationary state takes place when the arrival of fresh water at the discharge rate is balanced by the runoff of the freshened waters beyond the 10 km vicinity of the mouth**.** In contrast, in the case of an upwelling-type baroclinic current: the growth of ***Vol*** continues indefinitely.

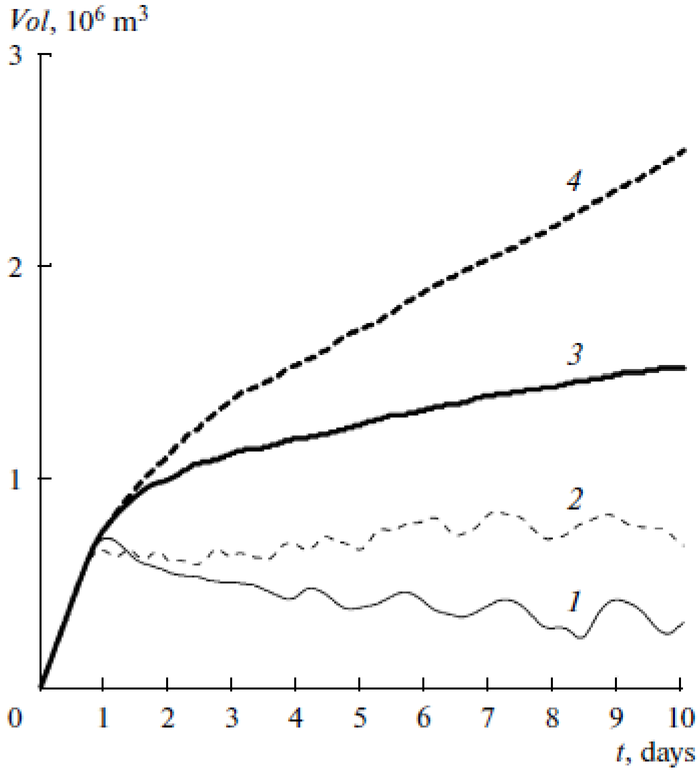

Figure 3: Dependence of the total volume of fresh water in the 10 km vicinity of the river mouth upon the time ***t*** of the source at an alongshore baroclinic current of the downwelling type (*1* and *2*) and the upwelling type (*3* and *4*) in the cases of flat bottom (*1* and *3*) and sloped bottom (*2* and *4*) basins

3. Surface-advected plume under wind forcing

3.1 Lagrangian model of a plume

We develop here a Lagrangian approach based on tracking the motion and dissipation of individual "particles" of the river water discharged into the sea. The particles are released from the river mouth, separated by regular time intervals and assigned with the initial velocity depending on the discharge rate. The module and direction of the velocity are set to randomly fluctuate around the mean values. The number of the particles appearing during a time step of the integration is proportional to the river inflow velocity at the step.

The subsequent motion of the particle is determined by the momentum equation applied to this specific particle. The overall set of particles defines the river plume and hence the evolution of the plume structure is obtained. We presume that the buoyant plume remains confined to the surface layer, therefore, the model considers the 2D-motion of the particles, although the water belonging to the particle is allowed to vertically mix with the underlying sea water, so that the salinity and density change in time until the particle eventually dissipates. At every step of the computation, the model reads the corresponding values from the input time series of river discharge rate, wind stress, and ambient sea current velocity data. The following forces are applied to the individual particle: the Coriolis force, the pressure gradient force, the wind stress force, the friction at the lower boundary of the plume, and the lateral friction. The model then calculates the acceleration components at every time step.

In order to simulate the small-scale horizontal turbulent mixing, the deterministic approach described above was complemented by the following random-walk scheme:

$$x^{i+1} = x^i + v_x^i \Delta t + \sqrt{2D_h \Delta t}\,\eta_x \; ; \; y^{i+1} = y^i + v_y^i \Delta t + \sqrt{2D_h \Delta t}\,\eta_y$$

where **(x,y)** are the coordinates of an individual particle, **(v_x,v_y)** are the average velocity components of a particle during the i-th time step, **Δt** is the time step, **D_h** is the horizontal diffusion coefficient depending on the velocity field as specified below, and **(η_x,η_y)** are the independent random variables with standard normal distribution, which were produced by a random number generator. This approach that combines deterministic description of the motion with a stochastic random-walk scheme was used in a number of previous works, mainly for simulating the transport of pollutants (Korotenko, 1994; Mestres et al., 2003; Lardner et al., 2006).

As the salty water from below is entrained into the plume gradually replacing the fresh water, the height of the elementary column in the plume decreases, while the density of water in it increases according to the linear equation:

$$\frac{\partial h}{\partial t} = -D_v$$

The horizontal and vertical diffusion coefficients used in the equations were calculated from the following formulas:

$$D_h = \zeta_h \sqrt{\left(\frac{\Delta u_x}{\Delta x}\right)^2 + \frac{1}{2}\left(\frac{\Delta u_y}{\Delta x} + \frac{\Delta u_x}{\Delta y}\right) + \left(\frac{\Delta u_y}{\Delta y}\right)^2} \left[\frac{m}{s}\right],$$
$$D_v = \zeta_v (1 - \min\,(1, Ri)^2)^3 \left[\frac{m}{s}\right],$$

where ζ_h, ζ_v are the horizontal and vertical dimensionless scaling coefficients, $Ri = \frac{N^2}{S^2}$ is the Richardson number, $N = \sqrt{\frac{g}{\rho}\frac{\rho_{sea} - \rho}{\Delta z}}$ is the buoyancy frequency, S is the vertical shear. The former relation is the well-known Smagorinsky formula (Smagorinsky, 1963), while the latter one was adopted from (Large et al., 1994).

The parameterization of the vertical diffusion through the Richardson number seems to be physically adequate in this case. Indeed, the vertical mixing beneath the plume should be mainly governed by two competing processes: on the one hand, the shear between the plume easily moving under the wind forcing and the underlying sea water tends to increase mixing. On the other hand, the enhanced vertical stratification tends to damp it. The ratio between the two mechanisms is quantified by the Richardson number.

The boundary conditions at the coastline were formulated as the no-normal flow condition, i.e., once the particle hits the shore, its cross-shore velocity component vanishes, while the along-shore component is retained without change, that is, the lateral boundary friction was neglected.

3.2 Validating the model

The set of model validation experiments consisted in simulations of the Mzymta River plume under the "real" conditions during the two periods, namely, May 26-30, 2010, and May 27-31, 2011. Although Mzymta is the biggest river of Russia feeding the Black Sea, it is relatively small with its catchment area of 885 km^2, discharge rate of 49 m^3/s on the long-term average, and mean annual runoff of about 1.6 km^3. The data used as the input for the model were the observational series of the wind stress, river discharge rate, ambient current velocity, as obtained from the field measurements at 10 min intervals. The observed plume configurations on the first days of the simulation experiments, i.e., May 26, 2010, and May 27, 2011, were prescribed as the initial conditions.

In order to validate the model, the "snapshots" of the simulated plume corresponding to the noon of every day during the simulation period were compared to those obtained from the in situ and satellite observations. As illustrated by Figs. 4a,b, the position, pattern, and area of the modeled plume for the simulation periods in May, 2010, and May, 2011, generally, agreed well with those observed on the respective days. Hence, the series of validation experiments described in this section demonstrated that the model is capable of reproducing the plume rather realistically, at least, under the conditions of moderate forcing.

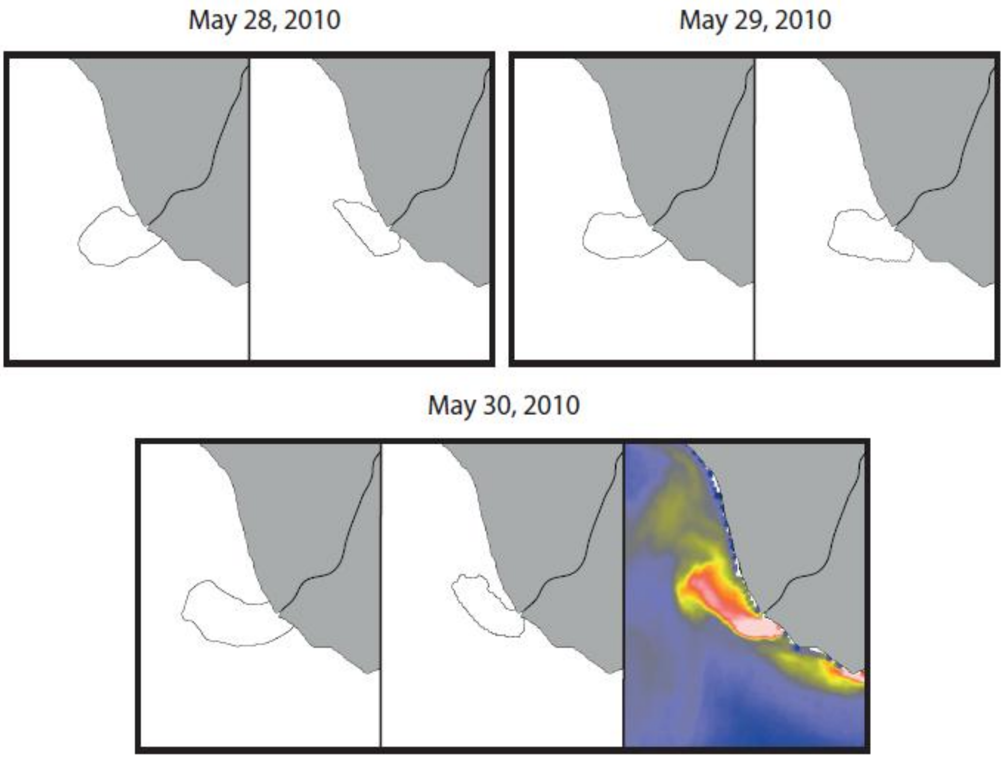

(a)

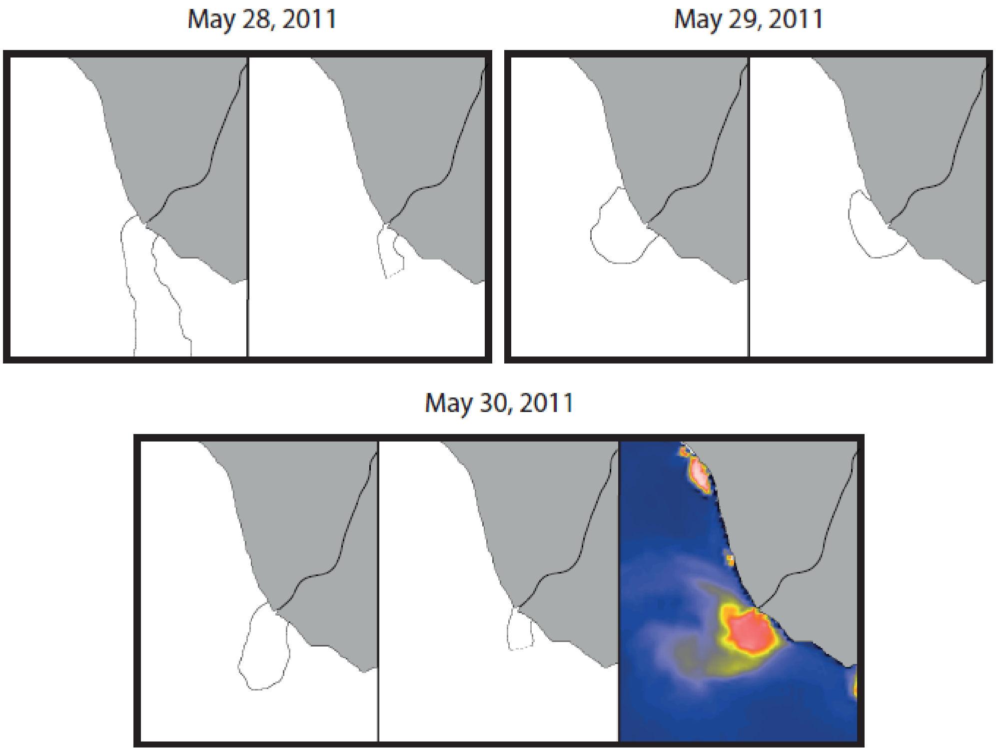

(b)

Figure 4: Mzymta River plume contours modeled under "real" conditions ("m"), in situ observed plume contours ("o") and satellite images of the plume ("s") during the periods May 28-30, 2010 (a), and May 28-30, 2011 (b). The dashed lines do not correspond to the real plume borders, and only indicate the southernmost part of the ship track.

3.3 Dependence of plume on wind stress

Wind forcing is the most important external factor that affects the area, shape and orientation of the plume. A number of previous observational and modeling investigations addressed this issue (Bowman, 1978; Bowman and Iverson, 1978; Chao, 1988; Fennel and Mutzke, 1997; Pullen and Allen, 2000; Janzen and Wong, 2002; Jonson et al., 2003; Hetland, 2005; Choi and Wilkin, 2006; Hunter et al., 2006; Whitney and Garvine, 2006). However, most of those dealt with either the specific measured winds or some illustrative idealized cases. No generalized understanding of the plume dependence on the wind forcing applied in different directions (with respect to the shoreline and river mouth) has been achieved. In this part of the study, we investigate this dependence using the model. Low computational cost of the Lagrangian model enabled us to perform the total of over 5000 simulation runs, changing the wind speed and direction with small increment from one run to another.

We simulated plume spreading under four "archetypal" wind forcing regimes, namely, the onshore, offshore, and the two alongshore wind directions. Once again, we refer to the alongshore wind blowing to the right of the mouth as "downwelling-favoring", and the alongshore wind blowing to the left of the mouth as "upwelling-favoring". The river discharge rate was kept constant during each run. The four resulting plots expressing the dependence between the plume area and the wind stress are shown in Fig. 5. Two of these graphs, namely. those corresponding to the downwelling-favoring and the offshore winds, are very similar. The plume area initially increases with the wind stress and attains certain maximum value. Further growth of the wind stress reduces the plume area, and eventually destroys the plume completely. On the contrary, the dependencies for the two others "archetypal" winds are different from this pattern, as well as from each other. The growth of the onshore wind stress causes continuous, albeit not uniform, decrease of the plume area, while the increase of the "upwelling-favoring" wind results in initial decrease of the plume area, followed by an intermittent increase and then eventual decay of the plume.

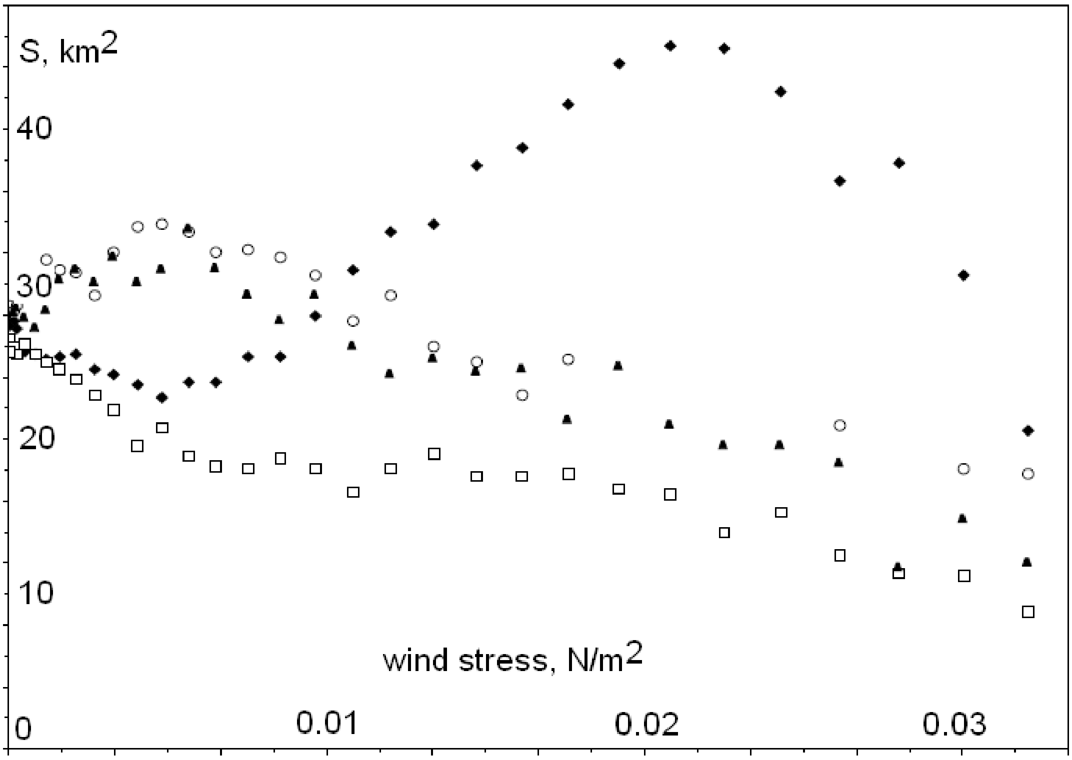

Figure 5: Modeled plume area as a function of wind stress magnitude for four "archetypal" wind forcings at t=1000 min, river discharge velocity 0.42 m/s. Onshore wind (squares), offshore wind (triangles), downwelling-favorable wind (circles), upwelling-favorable wind (diamonds).

The notably different shapes of the curves expressing the dependencies of the plume area on the wind stress for different wind directions raise the question of the mechanisms behind. First of all, we note that, regardless of their direction, sufficiently strong winds should destroy the plume due to enhancing vertical and horizontal mixing. Therefore, all the curves should tend to zero in the limit of high wind stress values, which is indeed the case. However, the behavior is less obvious in the low and intermediate wind stress ranges. Geometrically, the four archetypal winds can be identified for any estuary: two blowing perpendicular to the shore (onshore and offshore), and the other two blowing along the shore (one to the left of the initial momentum of the river water, which we call "upwelling-favoring", and the "downwelling-favoring" one opposite to it). In the region of this study, these four basic wind directions are represented by the respective SW, NE, NW, and SE winds. We now speculate that the water particles in a freely propagating, unforced plume naturally tend to move offshore because of their inertia, and along the shore to the right/left of the estuary (for the Northern/Southern hemisphere) because of the Coriolis force. Further, if the wind forcing is applied, the wind drag can act either in favor or against these "preferred" directions.

For example, both the offshore and the "downwelling-favoring" alongshore winds produce drags that are congenial with the free motion of the plume. Therefore, as long as the wind stress is not strong enough to destroy the plume, it facilitates its spreading, and the plume area initially increases with τ. As the wind stress grows further, the dissipation increases, so the plume area attains its maximum value at some critical $\boldsymbol{\tau}_{\mathbf{cr}}$, and then starts to decrease.

In contrast with the winds of the directions mentioned in the preceding paragraph, the onshore wind is always against the natural propagation of the plume. It presses the plume towards the coast and tends to arrest it within a narrow belt adjacent to the shore. The wind-induced dissipation adds to the decay of the plume. Therefore, under the conditions of the onshore wind stress, the area of the plume decreases steadily, though not linearly.

.

The most complex dependence on the wind stress module is evident for the "upwelling-type" winds whose drag is also against the free motion of the plume. Once such a wind is applied to the initial "bulge-shaped" plume, its action is manifested in a retreat of the "downstream", far edge of the plume towards the river mouth. At the same time, the water particles forming the "upstream" edge of the plume near the mouth are less sensible to the wind due to their higher initial momentum, stronger Coriolis force, and, especially, larger vertical extent of the plume layer. Therefore, as long as $\boldsymbol{\tau}$ is relatively small, the "upstream" edge remains almost intact, while the "downstream" one displaces towards the mouth, and the plume initially narrows and attains a minimum area, as reflected in the left portion of the corresponding curve. However, if the wind stress grows further, the entire plume is eventually forced to migrate to the left of the river mouth and stretches with the wind, so its spatial extent starts to increase with $\boldsymbol{\tau}$**.** Finally, as the growth of the wind stress continues, the dissipation prevails and the plume vanishes.

4. Conclusions

In this paper, we described numerical experiments with two different hydrodynamic models aimed at investigating the response of the buoyant river plumes to the wind forcing and their interactions with the coastal baroclinic circulations.

It is established from the experiments with POM that the alongshore baroclinic upwelling-type and downwelling-type currents transport the sea-entering river runoff in different ways. The pattern of the baroclinic downwelling-type current turns out to be much simpler and looks as follows. The isopycnals in the area of the coastal baroclinic downwelling-type current exhibit descent in reference to the undisturbed state, so that the density front at the sea surface does not appear (or appears only slightly) at the sea surface. Therefore, the incoming river water is easily entrained into the coastal baroclinic current and transported by the latter. On the other hand, a relatively broad shore-touching plume of freshened water forms to the right of the mouth with the core of the baroclinic current occurring inside the plume.

The pattern of the river water transport by the alongshore baroclinic upwelling-type current appears more complicated. Firstly, the isopycnals in the domain of the coastal baroclinic upwelling-type current tend to ascend onshore (in reference to the undisturbed state), which results in the appearance of a sharp density front at the surface. The latter serves as a barrier preventing the offshore dispersal of the freshened waters. As a result, a relatively narrow plume of freshened waters forms adjacent to the shore to the left of the mouth (i.e., along the background current). The plume is limited by a density front related to the baroclinic current, whose core occurs at the offshore side of the plume. With the transport to the left along the background baroclinic current part, a fraction of the fresh water runoff is transported alongshore to the right in a process similar to the geostrophic adjustment in the absence of the background currents. Eventually, the entire coastal vicinity of the mouth becomes filled with the freshened water. In consequence, a considerably larger volume of river water can be accumulated in the mouth's vicinity in the presence of the upwelling-type current as compared to the case of the downwelling-type one. For instance, our numerical experiments revealed that the river water volume accumulating in the 10 km vicinity of the mouth under the background baroclinic upwelling-type current is about 3 times as large as the volume corresponding to the downwelling-type current.

To illustrate this inference with the field observations, we take advantage of the measurement data from our survey of 2008 in the plume of the Vulan River. This is a small river with the average runoff of about 10 m^3/s (which roughly corresponds to the conditions of our numerical experiment), and the characteristic size of the plume is no more than one kilometer. Fig. 6 displays some results of these measurements. The arrows represent the vectors of the wind stress. The shore line in this part of the Black Sea passes from the northwest to the southeast so that the northwesterly winds correspond to the upwelling conditions, while the downwelling conditions are associated with the southeastern winds. The anomaly $\boldsymbol{\Delta S}$, designated with circles in the figure, is the difference of the salinity within the plume and the background salinity of the waters outside the plume. It is easy to see that, even under the conditions of a downwelling-type wind, the respective salinity anomaly tends to zero, which means the dilution of the plume over a large area. On the contrary, the salinity anomaly in a plume is well-marked under even weak upwelling-type winds.

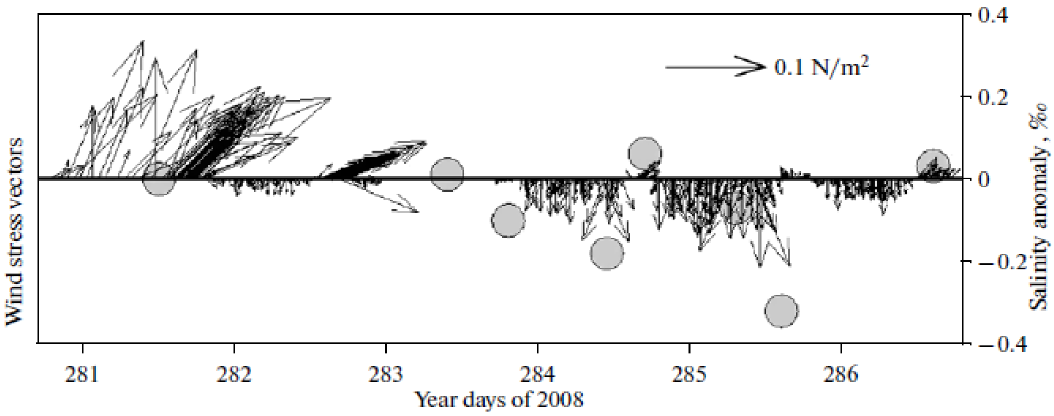

Figure 6: Time series of the wind stress vectors (arrows) and salinity anomalies (grey circles) in the area adjacent to the mouth of the Vulan river (the Russian coast of the Black Sea) according to our measurements in October of 2008. The strongest salinity anomalies in the estuary occurred under the conditions of the upwelling-type wind of northern rhumbs. On the contrary, the river plume happens to be washed out and the salinity anomalies were virtually indistinguishable under the downwelling-type winds.

We also developed a Lagrangian model of a surface-advected river plume. Combining the deterministic approach based on the momentum budget with a random-walk scheme, the model reproduced satisfactorily the general features of the plume dynamics known from previous studies and the original in situ observations of the Mzymta River plume in the Black Sea. Using the model, we investigated the dependencies between the spatial extent of the plume and the wind stress. The character of these dependencies proved to depend critically on the wind direction. For the offshore and "downwelling-favoring" alongshore winds, the plume area initially grows with the increase of $\boldsymbol{\tau}$, and then starts to decrease when $\boldsymbol{\tau}$ exceeds certain critical value. For the onshore wind, the area decreases steadily (though not linearly) as $\boldsymbol{\tau}$ increases. The most complex behavior is observed for the "upwelling-favoring" alongshore wind: the plume area initially decreases until the wind stress exceeds a certain critical value, then starts to increase with $\boldsymbol{\tau}$ and attains a maximum, and then eventually drops to zero as $\boldsymbol{\tau}$ continues to increase. In this paper, we intentionally do not focus on the corresponding quantitative threshold values of $\boldsymbol{\tau}$, because those should be site-specific and may depend on the conditions of a concrete simulation. However, the qualitative dependencies revealed from these experiments should be of a more general applicability.

Acknowledgements This work was supported by Russian Academy of Sciences (Research Program 23) and the EU Framework Program 7 (CLIMSEAS Project).

REFERENCES

Blumberg A. F., L. A. Khan, and J. P. St. John, 1999: Three-dimensional hydrodynamic model of the New York Harbour region. *Journal of Hydraulic Engineering,* 125:799-816.

Bowman, M. J., 1978: Spreading and mixing of the Hudson river effluent into the New York Bright. *Hydrodynamics of Estuaries and Fjords.* J. C. J. Nihoul (ed.), Elsevier, 373-386.

Bowman, M. J. and R. L. Iverson, 1978: Estuarine and plume fronts. *Oceanic Fronts in Coastal Processes.* M. J. Bowman and W. E. Esaias (eds.), Springer-Verlag, 87-104.

Chao, S.Y., 1988: River-forced estuarine plume. *Journal of Physical Oceanography*, 18:72-88.

Chao, S.Y. and W. G. Boicort, 1986: Onset of estuarine plumes. *Journal of Physical Oceanography*, 16:2137-2149.

Choi, B. J. and J. L. Wilki*n*, 2006: The effect of wind on the dispersal of the Hudson River plume. *Journal of Physical Oceanography*, 37:1878-1897.

Garvine, R.W., 1987: Estuary plumes and fronts in shelf waters: A layer model. *Journal of Physical Oceanography*, 17:1877-1896.

Garvine, R.W., 1995: A dynamical system of classifying buoyant coastal discherges. *Continental Shelf Research, 15:1585-1596.*

Garvine, R.W., 2001: The impact of model configuration in studies of buoyant coastal discharge. *Journal of Marine Oceanography,* 59:193-225.

Geyer, W. R., R. C. Beardsley, J. Candela, S.J. Lentz, R. Limeburner, W. E. Johnes, B. M. Castro, and I. D. Soares, 1996: Physical oceanography of the Amazon shelf. *Shelf Research, 16:575-616.*

Geyer W. R., P.Hill, T. Milligan, and P. Trykovski, 2000: The structure of the Eel River plume during floods. *Continental Shelf Research, 20:2067-2093.*

Hetland, *D. R.,* 2005: Relating river plume structure to vertical mixing. *Journal of Physical Oceanography*, 35:1667-1688.

Hunter, J. R., 1987: Application of Lagrangian particle-tracking technique to modeling of dispersion in the sea. *Numerical Modelling: Applications for Marine Systems.* J. Noye (ed.), North Holland, Amsterdam, 257-269.

Hunter, E., R. G. Chant, J. Kohut, L. Bowers, and S. Glenn, 2006: Sea breeze forcing on the New Jersey shelf. *Eos, Transactions, American Geophysical Union,* 87 (Ocean science meeting supplement). Abstract OS35J-01.

Janzen, C. D. and K. C. Won*g*, 2002: Wind-force dynamics at the estuary-shelf interface of a large coastal plain estuary. *Journal of Geophysical Research*, 107:3138.

Jonson, D. R., J. Miller, and O. Schofield, 2003: Dynamics and optics of the Hudson river outflow plume. *Journal of Geophysical Research*, 108:3323-3331.
Korotenko, K. A., 1994: The random walk concept in modeling matter transport and dispersion in the Sea. *Journal of the Moscow Physical Society*, 4: 335-338.
Lardner, R., G. Zodiatis, D.Hayes, and N. Pinardi, 2006: Application of the MEDSLIK oil spill model to the Lebanese spill of July 2006. *European Group of Experts on satellite monitoring of sea besd oil pollution.* European Communities. ISSN 1018-5593.
Large, W. G., J. C. McWilliams, and S. C. Doney, 1994: Oceanic vertical mixing: A review and a model with a nonlocal boundary layer parameterization. *Reviews of Geophysics, 32:363-403.*
Lentz, S. J. and R. Limeburner, 1995: The Amazon River plume during AMASSEDS: Spatial characteristics and salinity variability. *Journal of Geophysical Research*, 100:2355-2375.
Lvovich, M. I., 1986: *Water and Life* [in Russian]. Mysl, Moscow, USSR.
Mestres, M., J. P. Sierra, A. Sanchez-Arcilla, J. Gonzalez del Rio, T. Wolf, A. Rodriguez, and S. Ouillon, 2003: Modelling of the Ebro River plume. Validation with field observations. *Scientia Marina*, 67:379-391.
Munchow, A. and R. W. Garvine, 1993: Dynamical properties of a buoyancy-driven coastal current. *Journal of Geophysical Research*, 98:20063-20077.
Nash, D.B., 1994: Effective sediment-transporting discharge from magnitude-frequency analysis. *Journal of Geology*, 102:79-95.
Nash, J. D. and J. N. Moum, 2005: River plumes as a source of large-amplitude internal waves in the coastal ocean. *Nature*, 437:400-403.
Pullen, J. D. and J. S. Alle*n*, 2000: Modeling studies of the coastal circulation off Northern California: Shelf response to a major Eel River flood event. *Continental Shelf Research*, 20:2213-2238.
Simonov, A.I. and E. N. Altman, 1991: *Hydrometeorology and Hydrochemistry of the USSR seas*. *Volume 4*. Sensitivity to Change: Black Sea, Baltic Sea and North Sea. E. Ozsoy, A.
Simpson, J. H. and D. G. Bowers, 1984: The role of tidal stirring in controlling the seasonal heat cycle in shelf waters. *Annales Geophysicae*, 2(6):411-416.
Smagorinsky, J., 1963: General circulation experiments with the primitive equation. 1. The basic experiment. *Monthly Weather Review*, 91:99-165
Whitney, M. M. and R. W. Garvine, 2006: Simulating the Delaware Bay buoyant outflow: Comparison with observations. *Journal of Physical Oceanography*, 36:3-21.
Xia, M., L. Xie, and L. J. Pietrafesa, 2007: Modeling of the Cape Fear River estuary plume. *Estuaries and Coasts*, 30:698-709.
Yankovsky, A. E. and D. C. Chapman, 1997: A simple theory for the fate of buoyant coastal discharges. *Journal of Physical Oceanography*, 27:1386-1401.